How to cite: *Angew. Chem. Int. Ed.* **2023**, *62*, e202308273
doi.org/10.1002/anie.202308273

Gas-Phase Chemistry

Hydrogen-Atom Tunneling in a Homochiral Environment

*Fan Xie, Wenhao Sun, Beppo Hartwig, Daniel A. Obenchain, and Melanie Schnell**

Abstract: The role-exchanging concerted torsional motion of two hydrogen atoms in the homochiral dimer of *trans*-1,2-cyclohexanediol was characterized through a combination of broadband rotational spectroscopy and theoretical modeling. The results reveal that the concerted tunneling motion of the hydrogen atoms leads to the inversion of the sign of the dipole moment components along the *a* and *b* principal axes, due to the interchange motion that cooperatively breaks and reforms one intermolecular hydrogen bond. This motion is also coupled with two acceptor switching motions. The energy difference between the two ground vibrational states arising from this tunneling motion was determined to be 29.003(2) MHz. The corresponding wavefunctions suggest that the two hydrogen atoms are evenly delocalized on two equivalent potential wells, which differs from the heterochiral case where the hydrogen atoms are confined in separate wells, as the permutation-inversion symmetry breaks down. This intriguing contrast in hydrogen-atom behavior between homochiral and heterochiral environments could further illuminate our understanding of the role of chirality in intermolecular interactions and dynamics.

Tunneling, a fundamental phenomenon in quantum mechanics, enables particles to penetrate energy barriers that are insurmountable according to classical mechanics. This concept holds immense importance in chemical reactions,[1] biological processes,[2] and drug design[3] by facilitating faster reaction rates, specifically allowing light particles, like hydrogen atoms, to tunnel through energy barriers. The impact of hydrogen-atom tunneling is evident in various molecular processes, including acid-base reactions,[4] redox enzymatic catalyzed reactions,[5] and mutations in DNA.[6] The investigation of tunneling effects has opened the third paradigm to understand and even selectively control molecular reactions, beyond the perspectives and interpretations of conventional thermodynamics and kinetics.[7] In natural biological systems where most naturally occurring amino acids and sugars adopt a specific handedness, namely L-amino acids and D-sugars, respectively,[8] homochiral environments are more prevalent than heterochiral ones.[9] These two aspects taken together, quantum-tunneling phenomena and the dominance of homochiral environments, raise an interesting question about how hydrogen-atom tunneling dynamics differ in homochiral versus heterochiral surroundings.

To explore this, we employed homochiral and heterochiral dimers of *trans*-1,2-cyclohexanediol (CD) as a prototype to demonstrate the influence of different chiral environments on hydrogen-atom tunneling dynamics. The OH-stretching vibrations of the CD dimer and various other vicinal diol dimers were investigated using free-jet IR and Raman spectroscopy before, where a systematical characterization of the chiral recognition pattern, hydrogen-bond (H-bond) network, and intermolecular interactions were performed.[10] Nevertheless, there were no tunneling-related effects observed due to the comparatively low resolution (1 cm^{-1}) of the detection methods.

High-resolution vibrational and rotational spectroscopy is a widely recognized technique for providing unequivocal evidence of tunneling phenomena.[11] Through the combination with theoretical analysis, it allows for intuitive interpretations of various intermolecular and intramolecular tunneling dynamics such as torsional motions of concerted and free hydrogen atoms,[12] methyl-group internal rotations,[13] inversion motion of ammonia and amines,[14] and proton transfer.[15] For instance, the ring-polymer instanton method was utilized to derive the anti-gear and gear coupled tunneling motions observed for the water hexamer in its prism form, leading to an accurate reproduction of doublet-of-triplet splitting patterns observed in the experimental microwave spectra.[16] The double proton transfer dynamics in carboxylic acid hetero and homo dimers was extensively characterized by the combination of rotational spectroscopy and the flexible model.[17] Recently, microwave spectroscopy has revealed the influence of neighboring molecules on the proton transfer dynamics of the formic acid dimer,[18] which has been rationalized through solving the one-dimensional Schrödinger equation obtained from a simplistic ab initio computational procedure.[19]

In this study, we report the role-exchanging tunneling dynamics observed for a homochiral CD dimer using broad-

[*] Dr. F. Xie, Dr. W. Sun, Prof. Dr. M. Schnell
Deutsches Elektronen-Synchrotron DESY
Notkestr. 85, 22607 Hamburg (Germany)
E-mail: melanie.schnell@desy.de
Dr. B. Hartwig, Prof. Dr. D. A. Obenchain
Institut für Physikalische Chemie, Universität Göttingen
Tammannstr. 6, 37077 Göttingen (Germany)
Prof. Dr. M. Schnell
Institut für Physikalische Chemie, Christian-Albrechts-Universität zu Kiel
Max-Eyth-Str. 1, 24118 Kiel (Germany)

band chirped-pulse Fourier transform microwave (CP-FTMW) spectroscopy,[20] also known as Molecular Rotational Resonance (MRR) spectroscopy. The experimental results were complemented via an analysis based on the simplistic ab initio computational procedure employing a one-dimensional Schrödinger equation.[19] Our results have revealed a stark contrast in the hydrogen-atom dynamics for the ground vibrational states of these dimers between homochiral and heterochiral environments, which can have significant implications for our understanding of the role of chirality in intermolecular interactions and dynamics.

The microwave spectra were measured using the COMPACT (compact-passage-acquired coherence-technique) spectrometer,[21] which was operated in both the 2–8 and 8–12 GHz frequency ranges. Detailed information on the instrument's operation principle and settings has been previously published.[21–22] Here, a brief overview will be provided. A racemic sample of CD with a purity of 98%, obtained from Sigma–Aldrich, was used without any additional purification. The sample was placed in an internal reservoir close to the orifice of a pulsed valve and heated to 70 °C to increase its vapor pressure. Neon was utilized as a carrier gas with a backing pressure of 3 bars. The gas mixture was expanded supersonically into the vacuum chamber using the pulsed valve, resulting in the generation of complexes. The details of the data acquisition procedure are presented in the Supporting Information. In total, approximately four million acquisitions in the form of a free induction decay (FID) of the molecular coherence signal were recorded and averaged.

To assist in the interpretation of the microwave spectra and to systematically characterize the possible H-bonding configurations, extensive theoretical structure sampling was carried out. These calculations were performed using the scheme that combines the cost-effective ensemble sampling tool CREST[23] with subsequent geometry-optimization calculations. Structures within an energy window of 3 kcal·mol^{-1} generated by CREST (2.11.1) optimized with GFN2-xTB (6.1)[24] were reoptimized at the B3LYP-D3(BJ)/def2-TZVP[25] level of theory using the ORCA (5.0.3) computational package.[26] Harmonic frequency calculations were also performed to verify the presence of true minimum geometries and to provide zero-point-energy (ZPE) corrected energies.

In the racemic sample, both enantiomers of the CD monomer are present, namely S and R. Consequently, two distinct types of CD dimers can be formed during the jet expansion process, which are diastereomers with respect to each other. These dimers are classified as homochiral dimers, in which both monomer units exhibit the same chirality (RR and SS), and heterochiral dimers, where the two monomer units possess different chirality (RS and SR). To examine these formations, we conducted computations for both diastereomeric ensembles, specifically homochiral and heterochiral dimers. The comparative analysis of these two ensembles, along with the spectroscopic constants calculated for each, can be found in the Supporting Information Table S1.

In the IR and Raman spectroscopic study,[10c] four CD dimers including one heterochiral dimer and three homochiral dimers were detected in the helium free jet expansion. These observed dimers correspond to the minimum structures of Hetero-1, Homo-1, Homo-2, and Homo-3, as presented in Table S1. Hetero-1 adopts a S_4 symmetry resulting in zero dipole-moment components in all three principal axes, hence it is transparent to MW radiation. Homo-2 exhibits only a small dipole-moment component ($|\mu_b| = 0.6$ Debye), which can give rise to a (weak) microwave spectrum. In the present study, however, we did not detect Homo-2. Instead, Homo-1 and Homo-3 were assigned in the neon pulsed jet expansion. Of particular interest is the detection of Homo-3 that undergoes a tunneling motion, as indicated by the appearance of line splittings into doublets for all transitions, with an approximate splitting of 58 MHz. The characteristic a-type and b-type transition patterns are clearly visible in Figure 1 (a) and (b), respectively. In total, we were able to fit 122 transitions with the two-states Coriolis coupled semirigid-rotor Hamiltonian as shown in equation (1) using Pickett's spectroscopic fitting program.[27]

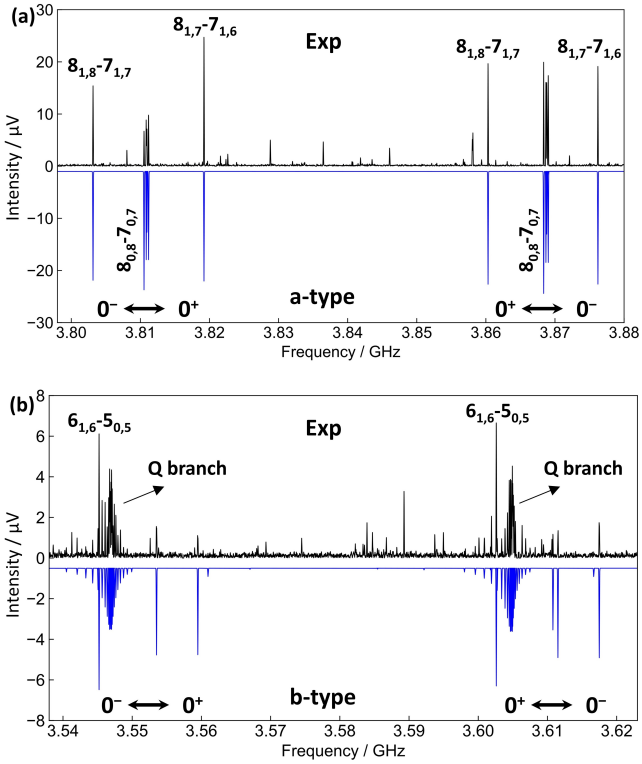

Figure 1. Sections of the broadband rotational spectrum highlighting the interstate transitions of the tunneling Homo-3. Black trace: experimental spectrum. Blue trace: simulated spectra based on the fitted spectroscopic constants. A rotational temperature of 1 K was used. The quantum numbers are defined using the standard nomenclature for the rotational energy levels of an asymmetric top, denoted as $J_{Ka,Kc}$. (a) a-type transitions from $J = 7$ to $J = 8$. (b) b-type transitions from $J = 5$ to $J = 6$ and the Q branch transitions.

$$H = \sum_i H_i^R + H_i^{CD} + \Delta E_{0^\pm} + F_{ab}\,(P_a P_b + P_b P_a) + F_{ac}\,(P_a P_c + P_c P_a) + F_{bc}\,(P_b P_c + P_c P_b) \quad (1)$$

Table 1: Experimental spectroscopic constants of Homo-3 and its comparison to the calculated minimum structure at the B3LYP-D3(BJ)/def2-TZVP level of theory. *N* is the number of transitions in the fit, and σ is the standard deviation.

	0^+	0^-	B3LYP-D3(BJ)
A/MHz	955.17086(54)	955.10899(54)	964
B/MHz	241.00516(14)	241.00432(14)	245
C/MHz	239.00913(86)	239.01158(9)	242
D_K/kHz	0.8106(65)		
D_{JK}/kHz	−0.1771(42)		
D_J/kHz	0.0281(5)		
d_1/kHz	0.0018(5)		
d_2/kHz	−0.7112(73)		
ΔE/MHz	29.003(2)		
F_{ab}/MHz	−4.7475(103)		
F_{ac}/MHz	−1.0646(129)		
F_{bc}/MHz	−0.20684(46)		
G_a/MHz	−0.9412(61)		
G_b/MHz	−0.2607(313)		
Dipole-moment comp./D	$\mu_a \approx \mu_b$, no μ_c		1.8/1.7/0.4
N	122		
σ/kHz	4.8		

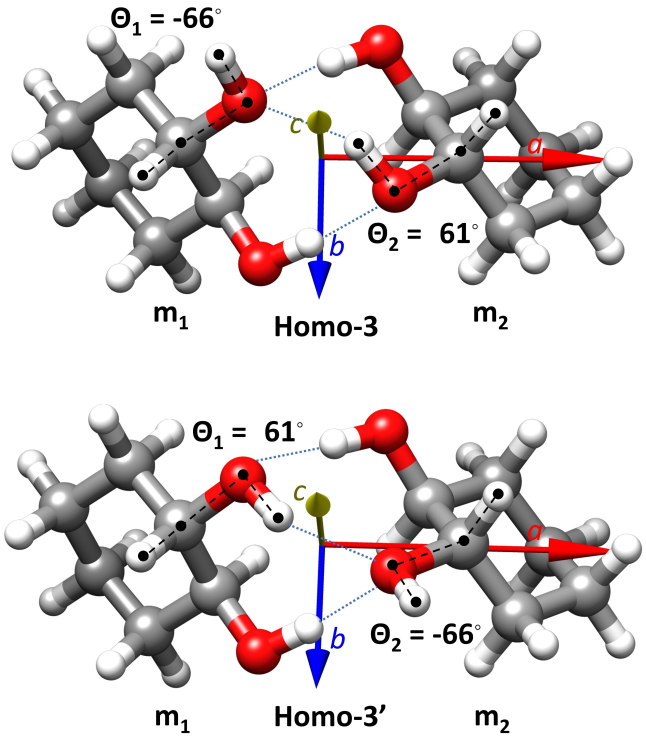

Figure 2. The two equivalent equilibrium structures Homo-3 and Homo-3′ optimized at the B3LYP-D3(BJ)/def2-TZVP level of theory. The principal axes *a*, *b*, and *c* are indicated with red, blue and yellow arrows, respectively. The dihedral angles Θ_1 and Θ_2 are associated with the torsional tunneling motion of the two hydrogen atoms that invert the sign of the dipole moment components along the *a* and *b* axes.

H_i^R is the rotational Hamiltonian for state i, here i corresponds to the two tunneling states 0^+ and 0^-. H_i^{CD} is the centrifugal-distortion contribution. $\Delta E_{0^\pm}$ is the energy difference between 0^+ and 0^-. F_{ab}, F_{ac}, and F_{bc} are the Coriolis coupling terms. P_a, P_b, and P_c are the angular momentum operators. The fitted spectroscopic constants are presented in Table 1. The list of all transitions included in the fit is presented in Table S3. For consistency, the determined spectroscopic constants and the list of included transitions of the non-tunneling Homo-1 are shown in Tables S2 and S4, respectively.

Based on the experimental rotational constants and spectral evidence of interstate transitions between 0^+ and 0^- vibrational states observed along the *a* and *b* principal axes, the corresponding equilibrium structure (Homo-3) and its energetic equivalence (Homo-3′) were identified from the calculated dimer isomeric ensemble (Table S1). As illustrated in Figure 2, Homo-3 is comprised of two CD monomer units (m_i, i = 1,2) connected by a network of three H-bonds. The main conformational difference between m_1 and m_2 stems from the orientations of two hydrogen atoms, marked by the dihedral angles $\Theta_1 = -66°$ and $\Theta_2 = 61°$, respectively. Conversely, in Homo-3′, these two hydrogen atoms have been reoriented, adopting $\Theta_1 = 61°$ and $\Theta_2 = -66°$. Essentially, the role of m_1 and m_2 in the H-bond network is exchanged upon the interconversion between Homo-3 and Homo-3′. This interconversion is achieved through the torsional motions of the two hydroxy groups, which break and reform an intermolecular H-bond via the interchange motion.[11k] Additionally, two acceptor switching motions are coupled to this vibrational motion. Collectively, these three motions contribute to the inversion of the sign of the μ_a and μ_b dipole-moment components, which is consistent with the equally spaced splittings observed for all a- and b-type transitions. Furthermore, the H-bond network motif of the minimum structure of Homo-3 exhibits a distinctive characteristic, featuring a pair of bifurcated H-bonds where both lone pairs of an OH group are involved in H-bonding interactions. This binding configuration sets it apart from all the other types of CD dimer structures depicted in Figure S1, where only one lone pair of the OH groups contributes to H-bond formation. Moreover, the minimum structure of Homo-3 aligns with the hom3′$_b$ homochiral dimer reported in the helium free-jet IR and Raman study.[10c]

In order to obtain a more comprehensive understanding of the homochiral concerted tunneling dynamics of two hydrogen atoms observed in the MW spectrum, we employed a recently developed simplistic computational procedure.[19] In this procedure, the harmonic ZPE-corrected minimum energy curve is calculated as well as the corresponding tunneling trajectories, vibrational eigenvalues, and wavefunctions of the large amplitude motion (LAM) by solving a one-dimensional Schrödinger equation using electronic energies and harmonic frequencies calculated at the B3LYP-D3(BJ)/def2-TZVP level of theory (see computational details in the SI). The obtained results are illustrated in Figure 3. The energetically equivalent Homo-3 and Homo-3′ were computed to be connected via a barrier

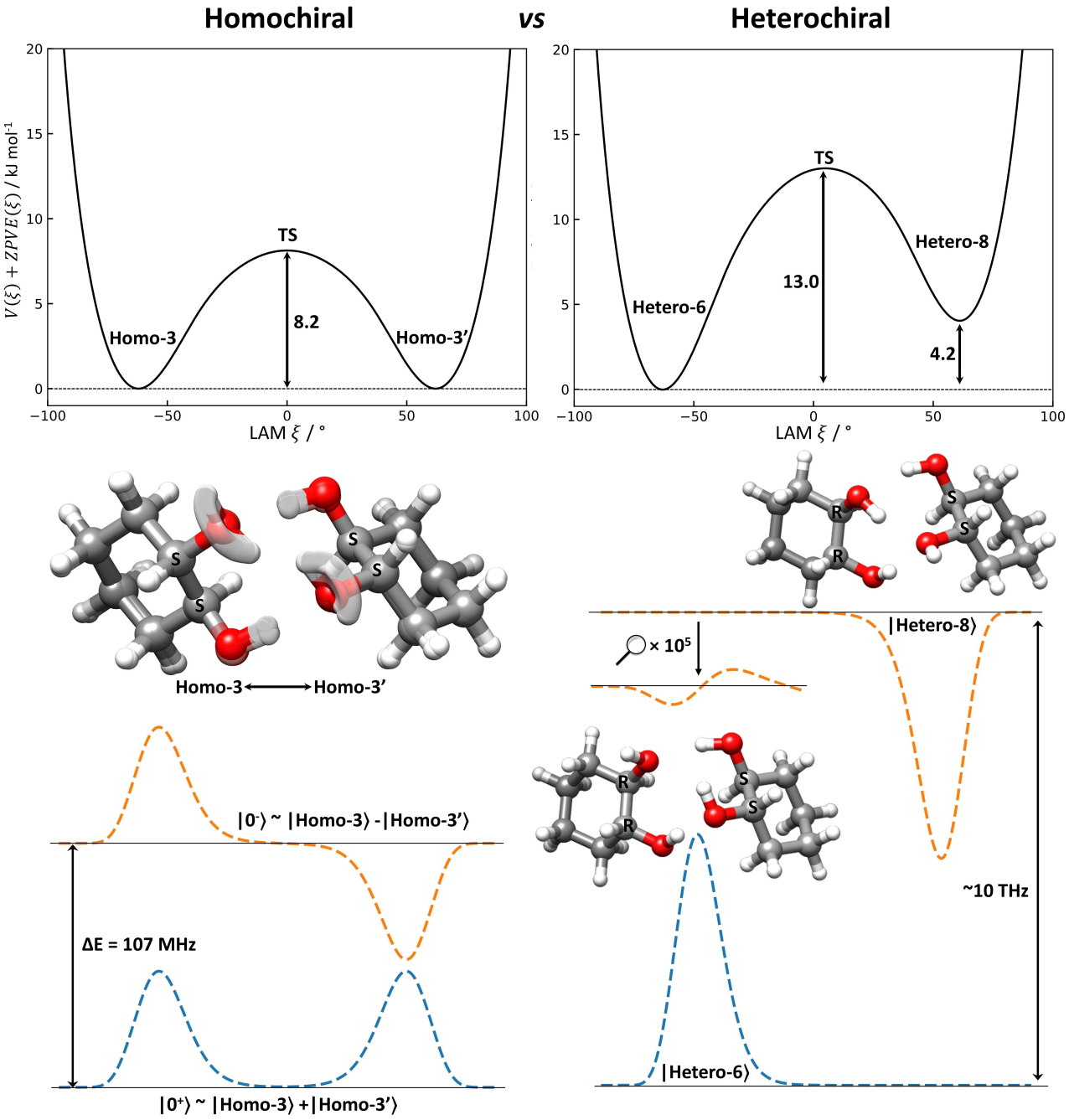

Figure 3. Solutions of the one-dimensional Schrödinger equation including vibrational eigenvalues and wavefunctions of the large-amplitude motion (LAM) for both the homochiral (left) and heterochiral dimer (right). The harmonic ZPE-corrected effective minimum energy surfaces are calculated at the B3LYP-D3(BJ)/def2-TZVP level of theory. The LAM coordinate is defined as $(\Theta_1 - \Theta_2)/2$.

of 8.2 kJ mol^{-1}. The interaction between the wavefunctions of these two equivalent minimum states results in the splitting of the ground vibrational state into two states, $|0^+\rangle$ and $|0^-\rangle$, with an energy difference ΔE of 107 MHz. It may not be a satisfying result compared to the experimental value of 29.003(2) MHz from the view of high-resolution spectroscopists. Nevertheless, considering that this one-dimensional model takes no empirical corrections from experimental spectra but only parameters from quantum-chemical calculations, the computed results are sufficient to provide a qualitative description of the tunneling dynamics. The square of the wavefunctions of $|0^+\rangle$ and $|0^-\rangle$ can be interpreted as the probability amplitude of finding the two tunneling hydrogen atoms at a specific point along the LAM trajectory. This probability amplitude can be intuitively visualized by plotting all possible hydrogen-atom coordinates, with the transparency adjusted proportionally to the absolute amplitude of the wavefunctions. As demonstrated,

the two tunneling hydrogen atoms exhibit the same probability of being a free hydrogen atom and a donor hydrogen atom. Their roles in the homochiral H-bond network can be exchanged via the cooperative double hydrogen-atom torsional motion.

Interestingly, when considering the hydrogen-atom dynamics in a heterochiral environment, two equilibrium structures are found in the heterochiral isomer ensemble (Table S1) that adopt a similar H-bond network to the observed tunneling Homo-3. However, since the monomer units in the heterochiral dimer are of opposite chirality, the permutation−inversion symmetry breaks down. The role-exchanging torsional motion of the two hydrogen atoms does not lead to energetically equivalent structures. Instead, two isomers Hetero-6 and Hetero-8, which differ by 4.2 kJ mol^{-1} in energy, were generated. They are connected by a barrier of 13.0 kJ mol^{-1}. The wavefunctions of the ground vibrational states |Hetero-6⟩ and |Hetero-8⟩ are well confined in the single potential well, and the interactions between them are calculated to be five orders of magnitude weaker compared to the strong wavefunction interaction in the homochiral dimer, as demonstrated in the zoomed-in section of the wavefunction of |Hetero-8⟩ shown in Figure 3.

With the consideration of thermodynamic properties of a molecular system, the hydrogen-atom dynamics plays an important role in determining the harmonic and anharmonic vibrational contributions to the molecular entropy.[28] Furthermore, it is important to highlight that the sharp contrasting behavior of hydrogen atoms in the homochiral and heterochiral dimers, as discussed above, represents not only a unique circumstance but is also found in CD dimers that adopt other hydrogen-bonding networks shown in the list of calculated isomers (Table S1). As depicted in Figure 4, the relative energy of the CD dimer isomeric ensemble illustrates the existence of two degenerate structures in each homochiral dimer, interconnected by the torsional motion of hydrogen atoms, which are presented in Figure S1. We did not observe a tunneling splitting for other homochiral dimers than Homo-3 as these tunneling dynamics involve cooperative motions of four hydrogen atoms resulting in breaking and reformation of three and even four H-bonds. Consequently, these cooperative motions result in higher interconversion barriers and overall heavier tunneling masses, leading to smaller values of ΔE. To provide a comparison, we performed the same simplistic computational procedure on Homo-1, yielding a calculated ΔE of 57 Hz. This value is significantly lower than our spectrometer resolution (25 kHz), which explains the absence of tunneling splittings in the experimental spectrum of Homo-1.

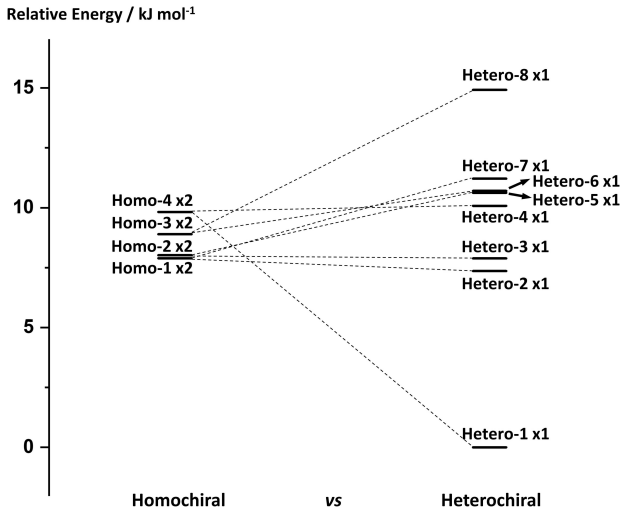

Figure 4. The *ZPE*-corrected relative energy diagram of homochiral and heterochiral CD dimers calculated at the B3LYP-D3(BJ)/def2-TZVP level of theory. Within an energy window of 10 kJ mol^{-1}, four homochiral isomers including Homo-3 exist. For each homochiral dimer, the isomer state is doubly degenerate. As for heterochiral dimers, the degeneracy is broken leading to eight isomers.

For the heterochiral dimers, conversely, two different isomeric states are generated for each heterochiral structure connected by the hydrogen-atom motions. From a thermodynamic perspective, this pronounced difference in the relative energy diagram coupled with hydrogen-atom dynamics could result in discernible entropy and free energy differences between homochiral and heterochiral molecular ensembles and ultimately affect their macroscopic properties such as specific heat capacity and solubility.[28]

In conclusion, concerted hydrogen-atom tunneling in homochiral environments has been investigated through a combination of broadband rotational spectroscopy and theoretical modeling using the homochiral dimer of CD generated in a cold molecular jet as a prototype. The double hydrogen-atom torsional motion that leads to the exchange of two monomer units was observed exclusively on the homochiral dimer. The results revealed a stark discrepancy in the hydrogen-atom dynamics and ensemble energy diagram between homochiral and heterochiral CD dimers, which plays an important role in determining the molecular entropies and free energies.[28b] These findings could shine light on our understanding of the role of chirality in chemical and biological systems, particularly in relation to the thermodynamic properties of a chiral molecular system. For example, conformational entropy regulates protein activities such as molecular recognition, enzymatic catalysis, and folding.[29] It is also worth to further investigate the possibly resolvable hydrogen-atom tunneling dynamics of other vicinal diol dimers. Examples include ethylene glycol, 2-methylpropane-1,2-diol, and pinacol with transient chirality where the bifurcated H-bond motif similar to the Homo-3 of CD dimer could be formed.[10e] Interesting factors that influence the hydrogen-atom tunneling dynamics could be discovered.

Acknowledgements

We acknowledge the detailed guidance of the simplistic ab initio computational procedure from Dr. Denis S. Tikhonov. F. X. acknowledges the support of an Alexander von Humboldt postdoctoral fellowship. This work has been supported by the collaborative linkage grant "Extreme light

for sensing and driving molecular chirality (ELCH)", SFB 1319, of the Deutsche Forschungsgemeinschaft (DFG). BH and DAO acknowledge the funding provided by the Deutsche Forschungsgemeinschaft —389479699/GRK2455. Open Access funding enabled and organized by Projekt DEAL.

Conflict of Interest

The authors declare no conflict of interest.

Data Availability Statement

The data that support the findings of this study are available in the supplementary material of this article.

Keywords: Chiral Recognition · Homochirality · Hydrogen-Atom Dynamics · Quantum Tunneling · Rotational Spectroscopy

[1] a) J. Meisner, J. Kästner, *Angew. Chem. Int. Ed.* **2016**, *55*, 5400–5413; b) P. S. Zuev, R. S. Sheridan, T. V. Albu, D. G. Truhlar, D. A. Hrovat, W. T. Borden, *Science* **2003**, *299*, 867–870; c) R. J. McMahon, *Science* **2003**, *299*, 833–834.
[2] A. Kohen, J. P. Klinman, *Chem. Biol.* **1999**, *6*, 191–198.
[3] a) A. B. Foster, *Trends Pharmacol. Sci.* **1984**, *5*, 524–527; b) T. Pirali, M. Serafini, S. Cargnin, A. A. Genazzani, *J. Med. Chem.* **2019**, *62*, 5276–5297.
[4] a) O. F. Mohammed, D. Pines, J. Dreyer, E. Pines, E. T. Nibbering, *Science* **2005**, *310*, 83–86; b) M. Rini, B.-Z. Magnes, E. Pines, E. T. Nibbering, *Science* **2003**, *301*, 349–352; c) B. Siwick, M. Cox, H. Bakker, *J. Phys. Chem. B* **2008**, *112*, 378–389.
[5] D. G. Truhlar, J. Gao, C. Alhambra, M. Garcia-Viloca, J. Corchado, M. L. Sánchez, J. Villà, *Acc. Chem. Res.* **2002**, *35*, 341–349.
[6] P. O. Löwdin, *Rev. Mod. Phys.* **1963**, *35*, 724.
[7] a) P. R. Schreiner, *J. Am. Chem. Soc.* **2017**, *139*, 15276–15283; b) P. R. Schreiner, H. P. Reisenauer, D. Ley, D. Gerbig, C.-H. Wu, W. D. Allen, *Science* **2011**, *332*, 1300–1303.
[8] a) N. Fujii, T. Saito, *Chem. Rec.* **2004**, *4*, 267–278; b) D. G. Blackmond, *Cold Spring Harb* **2010**, *2*, a002147.
[9] J. S. Siegel, *Chirality* **1998**, *10*, 24–27.
[10] a) B. Hartwig, M. A. Suhm, *Phys. Chem. Chem. Phys.* **2021**, *23*, 21623–21640; b) X. Aniban, B. Hartwig, A. Wuttke, R. A. Mata, *Phys. Chem. Chem. Phys.* **2021**, *23*, 12093–12104; c) B. Hartwig, M. Lange, A. Poblotzki, R. Medel, A. Zehnacker, M. A. Suhm, *Phys. Chem. Chem. Phys.* **2020**, *22*, 1122–1136; d) F. Kollipost, K. E. Otto, M. A. Suhm, *Angew. Chem. Int. Ed.* **2016**, *55*, 4591; e) "Diols under Investigation: Benchmarking their Monomers, Dimers and Chirality Recognition": B. Hartwig, Thesis, Georg-August Universität Göttingen, **2022**.
[11] a) L. Evangelisti, K. Brendel, H. Mäder, W. Caminati, S. Melandri, *Angew. Chem. Int. Ed.* **2017**, *56*, 13699; b) E. Zwart, J. Ter Meulen, W. L. Meerts, L. Coudert, *J. Mol. Spectrosc.* **1991**, *147*, 27–39; c) H. A. Harker, M. R. Viant, F. N. Keutsch, E. A. Michael, R. P. McLaughlin, R. J. Saykally, *J. Phys. Chem. A* **2005**, *109*, 6483–6497; d) D. P. Tabor, R. Kusaka, P. S. Walsh, E. L. Sibert, T. S. Zwier, *J. Phys. Chem. Lett.* **2015**, *6*, 1989–1995; e) K. Liu, M. Brown, C. Carter, R. Saykally, J. Gregory, D. Clary, *Nature* **1996**, *381*, 501–503; f) W. T. Cole, J. D. Farrell, D. J. Wales, R. J. Saykally, *Science* **2016**, *352*, 1194–1197; g) C. J. Gruenloh, J. R. Carney, C. A. Arrington, T. S. Zwier, S. Y. Fredericks, K. D. Jordan, *Science* **1997**, *276*, 1678–1681; h) C. Pérez, M. T. Muckle, D. P. Zaleski, N. A. Seifert, B. Temelso, G. C. Shields, Z. Kisiel, B. H. Pate, *Science* **2012**, *336*, 897–901; i) N. Pugliano, R. Saykally, *Science* **1992**, *257*, 1937–1940; j) F. N. Keutsch, R. J. Saykally, *Proc. Natl. Acad. Sci. USA* **2001**, *98*, 10533–10540; k) W. T. Cole, R. J. Saykally, *J. Chem. Phys.* **2017**, *147*, 064301.
[12] a) B. Velino, L. B. Favero, A. Maris, W. Caminati, *J. Phys. Chem. A* **2011**, *115*, 9585–9589; b) T. J. Lockley, J. P. I. Hearn, A. K. King, B. J. Howard, *J. Mol. Struct.* **2002**, *612*, 199–206; c) A. Maris, L. B. Favero, A. Vigorito, C. Calabrese, L. Evangelisti, S. Melandri, *J. Mol. Struct.* **2020**, *1205*, 127643; d) W. Caminati, *J. Mol. Spectrosc.* **1981**, *86*, 193–201.
[13] a) S. Khemissi, H. V. L. Nguyen, *ChemPhysChem* **2020**, *21*, 1682–1687; b) K. R. Nair, M. K. Jahn, A. Lesarri, V. V. Ilyushin, J.-U. Grabow, *Phys. Chem. Chem. Phys.* **2015**, *17*, 26463–26470; c) E. Hirota, *J. Chem. Phys.* **1966**, *45*, 1984–1990; d) R. Curl Jr, *J. Chem. Phys.* **1959**, *30*, 1529–1536; e) L. H. Spangler, *Annu. Rev. Phys. Chem.* **1997**, *48*, 481–510; f) H. V. L. Nguyen, W. Caminati, J.-U. Grabow, *Molecules* **2022**, *27*, 3948.
[14] a) A. Rauk, L. C. Allen, E. Clementi, *J. Chem. Phys.* **1970**, *52*, 4133–4144; b) J. Swalen, J. A. Ibers, *J. Chem. Phys.* **1962**, *36*, 1914–1918; c) B. Bleaney, R. Penrose, *Proc. R. Soc. London Ser. A* **1947**, *189*, 358–371; d) J. W. Simmons, W. Gordy, *Phys. Rev.* **1948**, *73*, 713; e) W. E. Good, *Phys. Rev.* **1946**, *70*, 213; f) M. Kréglewski, F. Winther, *J. Mol. Spectrosc.* **1992**, *156*, 261–291; g) N. Ohashi, S. Tsunekawa, K. Takagi, J. T. Hougen, *J. Mol. Spectrosc.* **1989**, *137*, 33–46; h) R. Sugisaki, T. Tanaka, E. Hirota, *J. Mol. Spectrosc.* **1974**, *49*, 241–250.
[15] a) L. Hatherley, R. Brown, P. Godfrey, A. Pierlot, W. Caminati, D. Damiani, S. Melandri, L. Favero, *J. Phys. Chem.* **1993**, *97*, 46–51; b) N. Howard, A. Legon, *J. Chem. Phys.* **1987**, *86*, 6722–6730; c) S. L. Baughcum, Z. Smith, E. B. Wilson, R. W. Duerst, *J. Am. Chem. Soc.* **1984**, *106*, 2260–2265; d) N. Love, A. K. Huff, K. R. Leopold, *J. Phys. Chem. A* **2021**, *125*, 5061–5068; e) A. Legon, *Chem. Soc. Rev.* **1993**, *22*, 153–163.
[16] J. O. Richardson, C. Pérez, S. Lobsiger, A. A. Reid, B. Temelso, G. C. Shields, Z. Kisiel, D. J. Wales, B. H. Pate, S. C. Althorpe, *Science* **2016**, *351*, 1310–1313.
[17] a) W. Li, L. Evangelisti, Q. Gou, W. Caminati, R. Meyer, *Angew. Chem. Int. Ed.* **2019**, *58*, 859–865; b) G. Feng, L. B. Favero, A. Maris, A. Vigorito, W. Caminati, R. Meyer, *J. Am. Chem. Soc.* **2012**, *134*, 19281–19286; c) L. Evangelisti, P. Écija, E. J. Cocinero, F. Castaño, A. Lesarri, W. Caminati, R. Meyer, *J. Phys. Chem. Lett.* **2012**, *3*, 3770–3775; d) R. Meyer, *J. Mol. Spectrosc.* **1979**, *76*, 266–300.
[18] W. Li, D. S. Tikhonov, M. Schnell, *Angew. Chem. Int. Ed.* **2021**, *60*, 25674–25679.
[19] D. S. Tikhonov, *Struct. Chem.* **2022**, *33*, 351–362.
[20] a) G. B. Park, R. W. Field, *J. Chem. Phys.* **2016**, *144*, 200901; b) G. G. Brown, B. C. Dian, K. O. Douglass, S. M. Geyer, B. H. Pate, *J. Mol. Spectrosc.* **2006**, *238*, 200–212; c) G. G. Brown, B. C. Dian, K. O. Douglass, S. M. Geyer, S. T. Shipman, B. H. Pate, *Rev. Sci. Instrum.* **2008**, *79*, 053103.
[21] D. Schmitz, V. A. Shubert, T. Betz, M. Schnell, *J. Mol. Spectrosc.* **2012**, *280*, 77–84.
[22] M. Fatima, C. Pérez, B. E. Arenas, M. Schnell, A. L. Steber, *Phys. Chem. Chem. Phys.* **2020**, *22*, 17042–17051.
[23] a) S. Grimme, C. Bannwarth, P. Shushkov, *J. Chem. Theory Comput.* **2017**, *13*, 1989–2009; b) S. Grimme, *J. Chem. Theory Comput.* **2019**, *15*, 2847–2862; c) P. Pracht, F. Bohle, S. Grimme, *Phys. Chem. Chem. Phys.* **2020**, *22*, 7169–7192.
[24] C. Bannwarth, S. Ehlert, S. Grimme, *J. Chem. Theory Comput.* **2019**, *15*, 1652–1671.

[25] a) S. Grimme, S. Ehrlich, L. Goerigk, *J. Comput. Chem.* **2011**, *32*, 1456–1465; b) E. Caldeweyher, S. Ehlert, A. Hansen, H. Neugebauer, S. Spicher, C. Bannwarth, S. Grimme, *J. Chem. Phys.* **2019**, *150*, 154122; c) D. G. Smith, L. A. Burns, K. Patkowski, C. D. Sherrill, *J. Phys. Chem. Lett.* **2016**, *7*, 2197–2203; d) C. Lee, W. Yang, R. G. Parr, *Phys. Rev. B* **1988**, *37*, 785; e) A. D. Becke, *J. Chem. Phys.* **1992**, *96*, 2155–2160; f) F. Weigend, R. Ahlrichs, *Phys. Chem. Chem. Phys.* **2005**, *7*, 3297–3305; g) F. Weigend, *Phys. Chem. Chem. Phys.* **2006**, *8*, 1057–1065; h) R. A. Kendall, T. H. Dunning Jr, R. J. Harrison, *J. Chem. Phys.* **1992**, *96*, 6796–6806; i) T. H. Dunning Jr., *J. Chem. Phys.* **1989**, *90*, 1007–1023.

[26] a) F. Neese, *Wiley Interdiscip. Rev.: Comput. Mol. Sci.* **2012**, *2*, 73–78; b) F. Neese, *Wiley Interdiscip. Rev.: Comput. Mol. Sci.* **2022**, *12*, e1606; c) F. Neese, F. Wennmohs, U. Becker, C. Riplinger, *J. Chem. Phys.* **2020**, *152*, 224108.

[27] H. M. Pickett, *J. Mol. Spectrosc.* **1991**, *148*, 371–377.

[28] a) L. Chan, G. M. Morris, G. R. Hutchison, *J. Chem. Theory Comput.* **2021**, *17*, 2099–2106; b) P. Pracht, S. Grimme, *Chem. Sci.* **2021**, *12*, 6551–6568.

[29] a) L. Zídek, M. V. Novotny, M. J. Stone, *Nat. Struct. Mol. Biol.* **1999**, *6*, 1118–1121; b) J. A. D'aquino, J. Gómez, V. J. Hilser, K. H. Lee, L. M. Amzel, E. Freire, *Proteins Struct. Funct. Genet.* **1996**, *25*, 143–156; c) A. J. Doig, M. J. Sternberg, *Protein Sci.* **1995**, *4*, 2247–2251; d) S.-R. Tzeng, C. G. Kalodimos, *Nature* **2012**, *488*, 236–240; e) K. K. Frederick, M. S. Marlow, K. G. Valentine, A. J. Wand, *Nature* **2007**, *448*, 325–329.

Manuscript received: June 12, 2023
Accepted manuscript online: July 19, 2023
Version of record online: August 4, 2023